Liquid-Cell Transmission Electron Microscopy Observation of Two-Step Collapse Dynamics of Silicon Nanopillars on Evaporation of Propan-2-ol: Implications for Semiconductor Integration Density

Yuta Sasaki[*,1], *Tomoya Yamazaki*[2], *Yuki Kimura*[*,2]

[1] SCREEN Holdings Co., Ltd., 322 Furukawa, Hazukashi, Fushimi-ku, Kyoto, 612-8486, Japan

[2] Institute of Low Temperature Science, Hokkaido University, Kita-19, Nishi-8, Kita-ku, Sapporo, Hokkaido 060-0819, Japan

ABSTRACT Miniaturization of semiconductor devices has made structures more fragile, leading to potential collapses due to capillary forces during drying after wet cleaning. This has hampered the integration of transistors according to Moore's Law. We have developed a method for preparing nanopillars in a liquid cell and have successfully observed their collapse by means of a cross-sectional view in transmission electron microscopy. The dynamics of collapse as a result of capillary interactions involve two steps. First, the nanopillars collapse due to an imbalance of capillary forces caused by a difference in liquid levels at the gas–liquid interface. Secondly, a liquid pool formed between nanopillars maintains the collapsed state of the nanopillars through surface tension. The nanopillars recover on reimmersion in the liquid after the collapse. This

method is effective, and is expected to contribute to the continued development of miniaturization and three-dimensionality of semiconductors.

KEYWORDS: capillary interactions, collapse dynamics, nanostructures, in-situ observation, LC-TEM, semiconductors

INTRODUCTION

Moore's Law, proposed by Gordon Moore in 1965, is a rule of thumb that states that the number of transistors integrated in a single silicon chip doubles roughly every 18 months due to the miniaturization of semiconductor devices.[1] This increase in the number of integrated transistors has led to an increase in the amount of data that can be handled and to faster operation of devices.[2] This increase in the amount of data capable of being processed permits big-data analysis and, in recent years, has been applied to deep learning. In addition, as the performance of semiconductor devices has improved, their cost has become lower and high-performance devices such as smartphones have become widely available. In this way, the higher performance of semiconductor devices has made our lives more convenient, but barriers exist to further development. One such problem is the collapse of nanostructures due to capillary interactions during evaporation of cleaning solutions, a process that is exacerbated by increasing miniaturization of semiconductor devices and consequent weakening of nanostructures.[3–5] The collapse of nanostructures destroys their expected functions, so countermeasures are essential. To solve this problem, new drying techniques to prevent collapse have been developed, such as the addition of an auxiliary substrate,[6] the use of a liquid with a low surface tension to control the wettability of the substrate,[7,8] the reduction of capillary forces by electromagnetic-wave irradiation,[9] or the elimination of capillary forces by drying without the involvement of a liquid phase through sublimation or supercriticality.

[10,11] However, no effective solution has yet been established, and this problem might be one factor that makes it impossible to maintain Moore's Law.

Effects of capillary interactions are often seen in everyday life, for example in the aggregation of hairs, which occurs when the forces generated to reduce the surface area of a liquid exceed the bending stiffness of wet hairs due to capillary interactions.[12] Deformation of structures due to capillary interactions is also commonly observed in high-aspect-ratio structures, such as carbon nanotubes.[13–16] The deformation of nanostructures in semiconductors was first observed in microelectromechanical systems,[17] where a two-dimensional model consisting of a liquid film between rectangular walls showed that capillary interactions are the cause of the collapse of structures.[18–22] In the two-dimensional model, the Laplace pressure generated by the meniscus at a gas–liquid interface between the walls and the generation of differences in liquid level (leveling of liquid) due to capillary interactions are considered to be dominant factors in structural collapse.[18–22] Later, models have been proposed for three-dimensional structures[23,24] and for systems with liquid evaporation.[25] From another perspective, efforts to form nanostructure patterns by controlling capillary forces have been studied.[26–31] However, most of these models are based on static energy equilibrium, and there are few examples of dynamic studies. Consequently, little is known regarding the dynamics of the collapse of nanostructures due to capillary interactions.

The actual collapse dynamics of nanostructures is considered to be a result of complex phenomena that cannot be represented by a static model, due to the high degree of freedom of the liquid. For example, Taroni and Vella reported that a two-dimensional model of a liquid sandwiched between two elastic structures can adopt multiple equilibrium states.[32] It is therefore necessary to consider the dynamics of capillary interactions to understand the collapse dynamics of nanopillars. However, it is difficult to accurately model the complex collapse dynamics of

nanopillars due to capillary interactions. In studies on the collapse dynamics of nanopillars, in situ observation is a powerful tool for directly capturing the relevant phenomena. For example, Chandra and Yang observed the collapse behavior of micropillars due to capillary interactions of micropillars 7–9 μm in height and with a submicron width by means of scanning electron microscopy (SEM), and they showed that a theoretical model for the cluster size of the micropillars agreed with the experimental values.[23,24] Vrancken et al. conducted in situ transmission electron microscopy (TEM) observations by machining nanopillars directly on a solution cell, and they succeeded in capturing the collapse of nanopillars due to capillary interactions in a topside view and in developing a collapse model.[33] However, in these previous studies, the nanopillars were all observed from above and, consequently, the gas–liquid interface could not be directly observed. To understand the collapse dynamics of nanopillars due to capillary interactions more accurately, it is necessary to observe the dynamics of the gas–liquid interface. Therefore, in this study we have established a method for preparing a thin section containing nanopillars in a liquid cell without collapsing them, and have conducted in situ TEM observations of the collapse behavior of the nanopillars in a cross-sectional view in which the gas–liquid interface could be seen.

EXPERIMENTS

Figure 1 shows SEM images of the silicon substrate used in this experiment. On the silicon substrate, nanopillars were formed with a width of about 30 nm, a height of about 600 nm, and an aspect ratio of about 20. Note that, because the bottoms of the nanopillars were widened, they were slightly stronger than similar perfectly straight-sided nanopillars. Structures with such high aspect ratios tend to collapse on liquid drying. Initially, the nanopillars were regularly arranged, as shown in Fig. 1(a). When the nanopillars were wetted with propan-2-ol that was subsequently evaporated, they collapsed, as shown in Fig. 1(b).

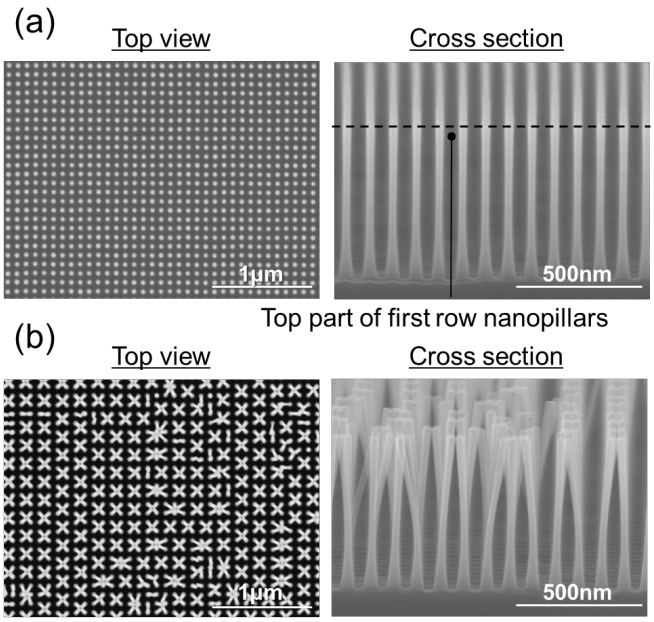

Figure 1. SEM images showing the structure of nanopillars used in the experiment and the collapse of nanopillars after evaporation of propan-2-ol. (a) SEM images of nanopillars in their initial state. Silicon nanopillars with a width of about 30 nm and a height of 600 nm were arranged on the silicon substrate with a pitch of about 90 nm. Therefore, the width of the spaces between the nanopillars was about 60 nm. (b) SEM images of nanopillars collapsed by evaporation of propan-2-ol.

Figure 2(a) shows an image obtained by in situ observation of the nanopillars by TEM (JEM-2100F; JEOL, Ltd., Tokyo). In most cases, when a solid sample is observed by TEM, it is inserted into a sample chamber under a high vacuum. If the sample is a liquid, it will evaporate when it is inserted into the sample chamber, so it is necessary to isolate liquid samples from the sample chamber to prevent their evaporation. We therefore used a Poseidon holder (Protochips, Morrisville, NC) in which the liquid sample is sealed between two silicon chips (a small silicon chip and a large silicon chip), permitting the liquid sample to be observed in isolation from the

sample chamber. Each of the two silicon chips has an observation window of amorphous silicon nitride through which the liquid sample can be observed. Therefore, if nanopillars are placed on the observation window of the smaller silicon, as shown in Fig. 2(b), they can be observed in a liquid phase.

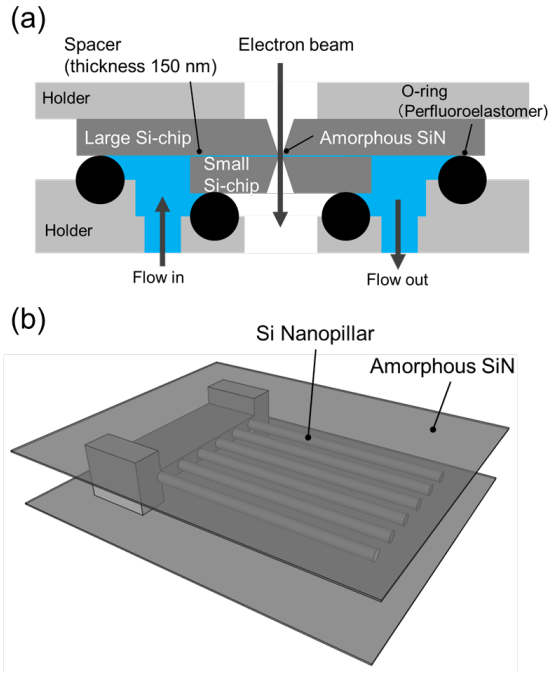

Figure 2. Schematic depiction of the nanopillars in the liquid. For the sake of clarity, the diagram is not drawn to scale. (a) The sample-fixation region of the Poseidon holder is shown. The sample was sealed between two silicon chips (a small Si chip and a large Si chip), and the small silicon chip had a 150-nm-thick spacer. There was an observation window of amorphous silicon nitride in the center of each silicon chip, and the electron beam was irradiated through the observation window. (b) Magnified view of the silicon nanopillars placed on the observation window of the small silicon chip and enclosed in the solution cell.

To observe the collapse behavior of the nanostructures by using the equipment shown in Figure 2, it was necessary to machine the nanopillars to a thickness that could be sealed in the solution

cell and to fix them onto the observation window of the small silicon chip. In addition, it was necessary to ensure that the nanopillars on the solution cell were not collapsed and there was no foreign matter between the nanopillars.

Focused-ion-beam (FIB) machining equipment is commonly used to fabricate thin sections for TEM observation, and it can machine substrates to a thickness of as little as several tens of nanometers (nanomachining). Normally, during FIB machining it is necessary to cover the machined area of a substrate with a protective film to prevent damage to the substrate surface due to beam flare. However, when a protective film is formed on nanostructures, it is deposited between the nanostructures. In this state, it is not possible to observe the liquid behavior between the nanostructures, so the protective film must be removed. Tungsten is generally used as a protective film because it is less susceptible to thermal effects of electron beams and less susceptible to machining by electron-beam flares. However, because tungsten is highly resistant to chemicals and heat, it is difficult to remove the protective film alone without causing damage to the nanostructures. We therefore searched for a suitable protective film that would protect the nanopillars during FIB machining, but which could be removed without damaging the nanopillars. As a result, we established a method involving the use of alumina as a protective film. Because alumina is highly heat resistant, it does not melt due to heating during FIB machining. In addition, alumina dissolves in hydrochloric acid, so it can be removed without damaging nanopillars after nanomachining. Moreover, alumina is commonly deposited by atomic layer deposition (ALD) and it can be deposited in narrow spaces of nanoscale dimensions.

Alumina was deposited on the silicon substrate with nanopillars by using an ALD system (R-200 Advanced; Picosun Oy, Masala). The precursor was trimethylaluminum, the oxidizing agent

was water, and the deposition temperature was 200 °C. The target thickness of the alumina film was 1.2 μm to ensure that the nanostructures were adequately covered.

A thin section of this substrate was machined by using FIB machining equipment (Hitachi High-Technologies FB2100). Figure 3 shows images obtained by scanning ion microscopy (SIM) during the machining process. First, a protective film of tungsten was formed on the alumina deposited on the Si substrate, as shown in Fig. 3(a), and the area around the protective film was roughly machined, as shown in Fig. 3(b). Next, the substrate was tilted to 60° and notches were formed from the sides, as shown in Fig. 3(c); these made it easier to cut thin section from the substrate later. Next, the thin section was thinly machined to a thickness of about 300 nm, and the central part of the thin section was further shaved to about 90 nm. The reason that the thickness of the central part was set to 90 nm is because the pitch of the nanopillar pattern was about 90 nm, so that there was one line of pillars in the central part. Depending on the machining position, there could have been two lines of pillars, so such a position is not discussed quantitatively. Figure 3(d) shows a SIM image of the thin section after machining. The thickness at the edge of the thin section was about 300 nm, and the thickness at the center was about 90 nm. Therefore, the distance between the nanopillars and the observation window was about 105 nm. The thicknesses of the edge and the center were changed to create a space between the observation window of the amorphous silicon nitride and the nanopillar when the thin section was sandwiched between solution cells, and to prevent contact between nanopillars and the observation window. Although the thickness of the edge of the thin section was 300 nm, which is thicker than the thickness of the spacer (150 nm), it was possible to sandwich the thin section without breaking the window, probably because of the flexibility of the amorphous silicon nitride observation window.

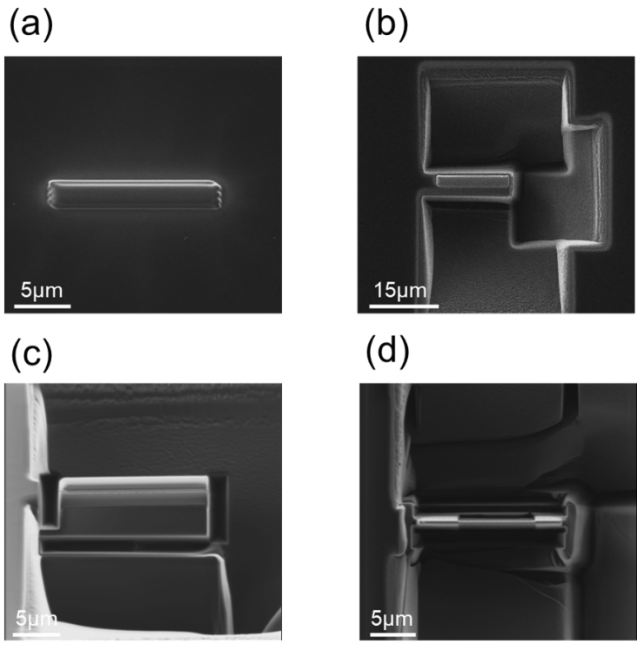

Figure 3. SIM image of the Si substrate being machined by FIB. (a) Deposited tungsten protective film on Si substrate. (b) After rough machining around the protective film. (c) After cutting into the thin film (60° tilted view). (d) The thin film after completion of all the machining.

The thin sections prepared by FIB were fixed onto the small silicon chip. There are several ways to lift out thin films. In this study, we adopted the pickup method using a micromanipulator (APS-001R; Micro Support Co., Ltd., Shizuoka), because ion-beam irradiation could break the observation window of the solution cell. Figure 4(a) shows an optical microscopy image of the thin section on the observation window of the solution cell. After lifting out the thin section on the silicon substrate (Fig. 3d) with a glass rod, the thin section attached to the tip of the glass rod was transported to the observation window of the solution cell and placed on the solution cell. If the thin section had just been placed on the observation window, it would have moved during observation in the liquid. We therefore used the tungsten-deposition function of the FIB to attach the thin film to the observation window. Figure 4(b) shows a SEM image (JEOL JEM-9320FIB)

of a tungsten-deposition trace connecting the thin section to the observation window of the solution cell. As shown in the magnified SEM image in Fig. 4(b), tungsten was deposited on the thin section and the observation window to prevent the thin film from peeling off the observation window. Figure 4(c) is a TEM image of the thin film placed on the solution cell, showing nanopillars near the center of the TEM image covered with alumina. Because the collapse of the nanopillars could not be observed under these conditions, the thin section was finally immersed in aqueous HCl at 110 °C to dissolve the alumina. When the alumina had dissolved, the nanopillars were stored in propan-2-ol until they were required for the experiments to prevent them from collapsing.

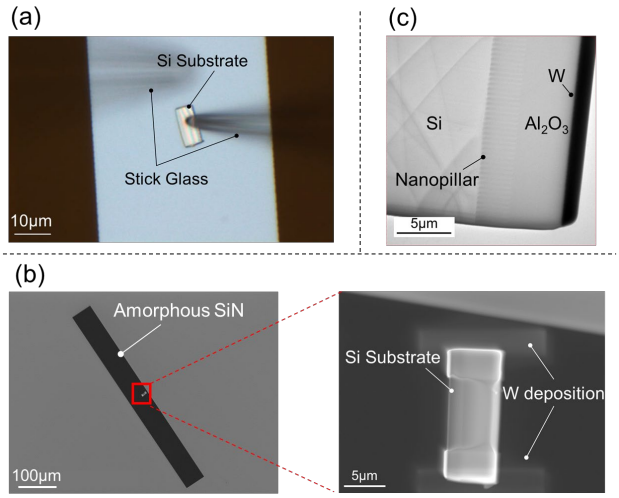

Figure 4. Fixation process of thin sections on the solution cell. (a) Optical microscopy image of a thin section placed on the observation window of the solution cell by a micromanipulator. (b) SEM image of the bonding trace connecting the thin section to the observation window. The thin section was fixed to the observation window by depositing tungsten across the thin section and the observation window. (c) TEM image of the thin section on the observation window of the solution cell.

The solution cell in which the thin section was placed was extracted from the propan-2-ol and assembled before the solvent evaporated. The Poseidon holder containing the solution cell was then inserted into the sample chamber of the TEM, and in situ observation was performed by using an electron beam with an acceleration voltage of 200 keV. The Poseidon holder has three ports for liquid flow. By opening these flow paths to the atmosphere, the liquid in the solution cell could be gradually evaporated.

RESULTS & DISCUSSION

Figure 5 and Supplementary Video 1 show the collapse of nanopillars due to evaporation of propan-2-ol. The TEM image in Fig. 5 at 0 s shows the nanopillars just before they collapsed. The nanopillars were wetted with propan-2-ol and did not collapse at 0 s. Interface 1 shown in the TEM image at 1 s was a gas–liquid interface of a liquid film formed between the nanopillars, and interface 2 was a gas–liquid interface of the liquid pool between the nanopillars and the observation window. The TEM image at 1 s shows that the space width between nanopillars has already changed at this point. A liquid film formed between the displaced nanopillars was observed (interface 1), and the interface formed a meniscus. The TEM image at 5 s shows that several nanopillars had collapsed at this stage. There was a difference in the liquid levels between that in the area where the space became wider and that where the space became narrower due to the displacement of the nanopillars.

The nanopillars are not considered to have been in contact with the observation window for two reasons. Firstly, interface 2 was located nearer the bottom than interface 1. The magnitude of the interaction between the two walls increases with cos θ, where θ is the contact angle between the liquid and the wall, and conversely decreases as the distance between the walls increases.[18] The

contact angle of propan-2-ol on the observation window is unknown, whereas the contact angle of propan-2-ol on the silicon wall is less than 5°.[34] On the other hand, because the distance between the nanopillars and the observation window was larger than the space width of the nanopillars, propan-2-ol must have sufficiently wetted the observation window for the nanopillars to have contacted the observation window. If the displacement toward the observation window was dominant and the nanopillar and the observation window were in contact, the distance between the observation window and the nanopillar would be less than the space width of the nanopillars, and interface 2 would be located nearer the tops of the nanopillars than interface 1 due to capillary interaction. However, the position of interface 2 in Figure 5 is well below that of interface 1, so the interaction between the nanopillars and the observation window is not considered dominant.

Secondly, the nanopillar is not out of focus. For the nanopillar to contact the observation window, it would need to be displaced by about 100 nm, which would be a sufficient displacement to cause it to become out of focus. However, these considerations do not prove that the nanopillars are not deformed toward the viewing window in the slightest. Further efforts are needed to perform a three-dimensional quantitative analysis.

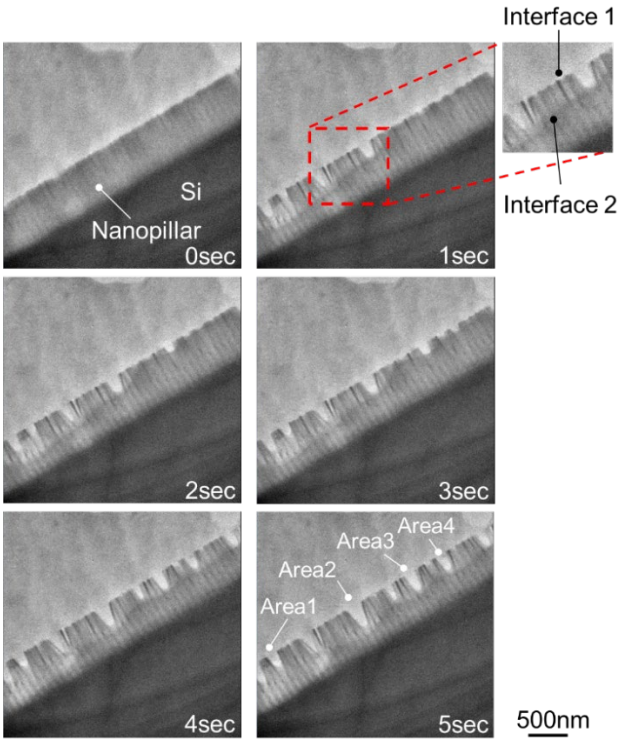

Figure 5. TEM images showing the collapse behavior of nanopillars due to evaporation of propan-2-ol. Propan-2-ol was evaporated by opening an inlet of the Poseidon holder at room temperature. Interface 1 is the gas–liquid interface of the liquid film formed between the nanopillars. Interface 2 is the gas–liquid interface of the liquid pool between the nanopillars and the observation window. The same observations are also shown in Supplementary Video 1.

Figure 6 shows the relationship between the space width and the difference in liquid level in each area described in Fig. 5 (at 5 s). In all areas, the space width increased as the difference in the liquid level increased. We believe that this occurs because the larger the difference in liquid level, the greater will be the difference in the Laplace pressure acting on the left- and right-hand sides of the nanopillars.[22] Because the liquid surface in the space adjacent to Areas 1–4 is located at the tops of the nanopillars, the difference in liquid level shown in Figure 6 corresponds to the

difference between the height of the liquid level in the adjacent space and that of the liquid level in Areas 1–4, respectively. Even at the same liquid-surface height, the space width differed by up to about 70 nm. This was probably because the effect of the depth direction was not taken into consideration. Even two-dimensionally arranged nanopillars in a space limited to a thickness of 150 nm can have different interfacial behaviors on each area. This demonstrates the difficulty of providing a quantitative analysis of the interfacial dynamics by using a simple two-dimensional model.

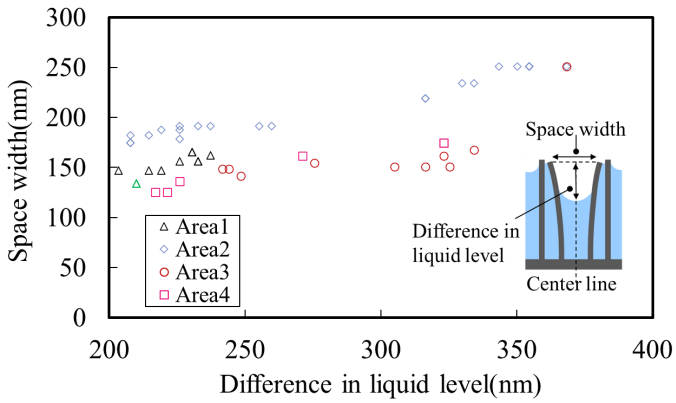

Figure 6. The dependence of the space width between the nanopillars on the difference in liquid level. The space width and the liquid-surface height of Areas 1–4 (shown in Fig. 5 at 5 s) were measured from the images and plotted. Areas 1–4 were selected because they had clear interfaces. The distance between the tops of two displaced nanopillars was defined as the space width, and the difference in liquid level was defined as the distance between the line connecting the tops of the nanopillars and the gas–liquid interface. The edge of the image was enhanced by using *Image J* software (National Institutes of Health, Bethesda, MA) before the distance was measured.

Phase 1 of Fig. 7 shows a conceptual diagram of the collapse dynamics of nanopillars due to capillary interactions, as shown in Fig. 5. When the liquid level fell below the top line of

nanopillars due to the evaporation of the liquid, a meniscus was formed at the gas–liquid interface between the nanopillars. Subsequently, the difference in liquid level increased due to capillary interactions, and the displacement of nanopillars increased, as shown in Fig. 6.

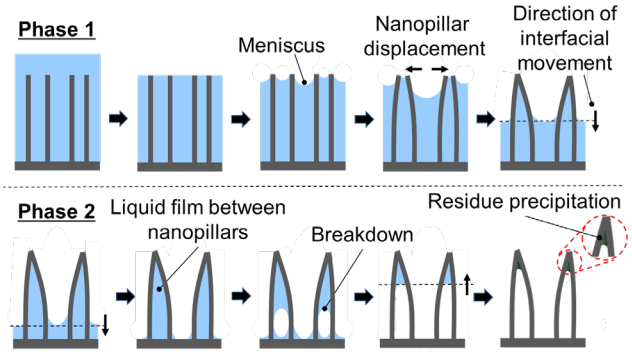

Figure 7. Conceptual diagram showing the dynamics of nanopillar collapse and liquid evaporation.

The collapse of nanopillars due to liquid evaporation can be described as a process in which nanopillars collapse (Phase 1) and a process in which the adhesion between nanopillars is maintained during liquid drying (Phase 2).

Figure 8 and Supplementary Video 2 show the evaporation behavior of the liquid pool formed between the collapsed nanopillars. As in Fig. 5, the state in which the gas–liquid interface is formed at the top of nanopillars is set to 0 s, and the TEM images from 0 to 3 s show the gas–liquid interface moving toward the bottom in the area where nanopillars were displaced and the space expanded. The liquid pool formed in the area where the space became narrower due to the displacement of nanopillars was maintained until the gas–liquid interface reached the bottom of the nanopillars. TEM images after 4 s show the evaporation behavior of the liquid pool formed in the narrowed space due to the displacement of nanopillars, and it is clear that the gas–liquid interface moved from the bottom of the nanopillars toward the top.

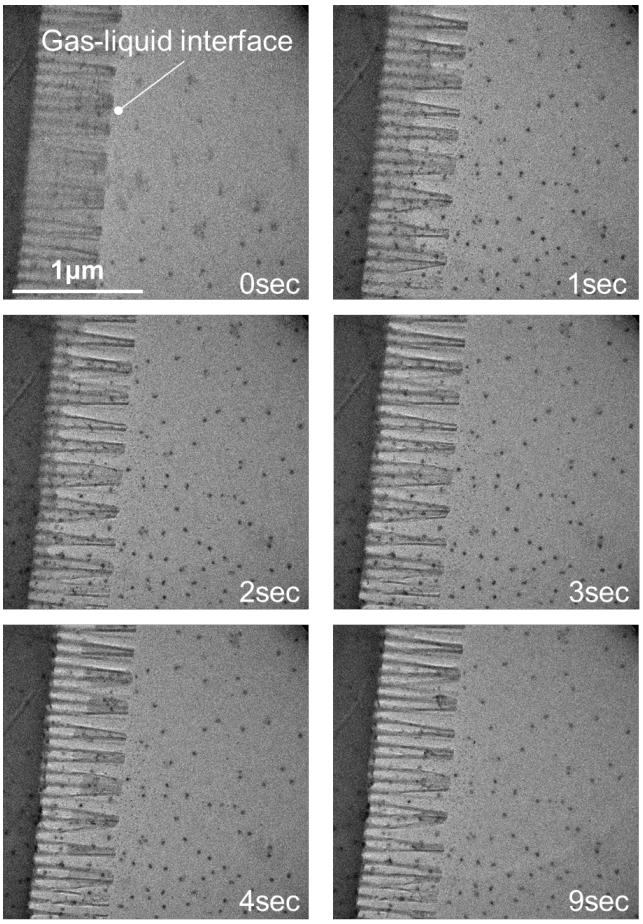

Figure 8. TEM images showing the drying behavior of propan-2-ol between nanopillars. TEM images show the drying of the liquid pool formed between nanopillars, and the interface at 0 s is the gas–liquid interface between propan-2-ol and air. The moment when the gas–liquid interface was at the top line of the nanopillars was set to 0 s. The black dots on the observation window are probably gold particles precipitated from propan-2-ol. If a solution cell with a gold spacer is used, gold particles may precipitate when the cell is irradiated with an electron beam. The same observations are also shown in Supplementary Video 2.

Phase 2 of Fig. 7 shows a conceptual diagram of the drying behavior shown in Fig. 8. After the collapse of the nanopillars, further evaporation of propan-2-ol causes leveling of the liquid due to

capillary interactions, and the liquid pool in the area where the space has expanded due to the displacement of nanopillars evaporates first. Subsequently, a liquid pool is left in the space between the collapsed nanopillars. Then, a gas–liquid interface is formed from the bottom of the substrate by evaporation of the liquid pool and this interface moves toward the top line of nanopillars. During this process, the nanopillars are thought to be maintained in a collapsed state by the surface tension of the liquid. The collapse behavior of nanopillars reported by Vrancken et al. corresponds to Phase 1 in Fig. 7.[33] Moreover, this is also similar to the behavior reported by Wie and co-workers, in which the top of micropillars contact each other.[35] In addition, the collapse behavior obtained from our observations indicates that the area where the liquid exists until the end is near the top of the nanopillars. Since the top of nanopillars is the part of the structure where the greatest torque is applied in the direction of displacement, capillary interactions work effectively to maintain the nanopillar in the collapsed state. If impurities are present in the droplet, they will be deposited near the adhesive surface, as shown in Phase 2 of Fig. 7, and the impurities will affect the maintenance of the collapsed state of the nanopillars.

Figure 9 and Supplementary Video 3 show nanopillars recovering on reimmersion in propan-2-ol after their collapse due to evaporation of propan-2-ol. Reimmersion was performed by injecting propan-2-ol from a syringe through the inlet of the Poseidon holder. The TEM images from 0 to 34 s mainly show the behavior of nanopillars immersed in propan-2-ol and the elimination of the leveling of liquid. The TEM images from 49 to 79 s show the recovery of nanopillars as the curvature of the meniscus decreased, and a comparison between the images at 0 s and 79 s shows that many of the collapsed nanopillars recovered. The reason why there is no image showing complete reimmersion in Figure 9 is that we could not control the complete reimmersion process. Even if we continued to inject propan-2-ol from a syringe through the inlet of the Poseidon holder,

the gas-liquid interface was stable at the top line of the nanopillars, as shown in the TEM image recorded at 79 s. This phenomenon is probably due to the balance between capillary forces and the surface tension force of propan-2-ol.

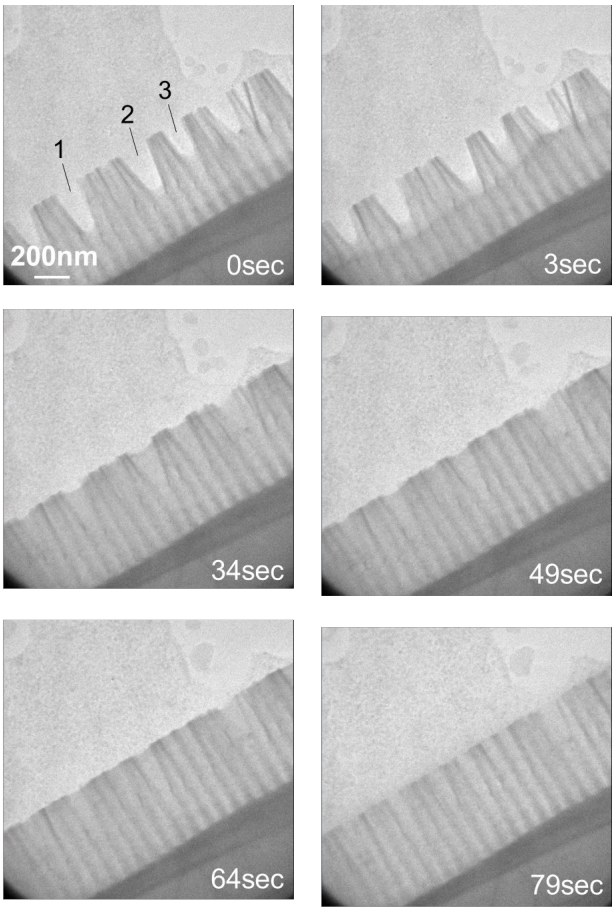

Figure 9. TEM images showing the recovery behavior of collapsed nanopillars when they were reimmersed in propan-2-ol. Reimmersion was performed by injecting propan-2-ol at a flow rate of 2 μL/min at room temperature from a syringe through the inlet of the Poseidon holder about 30 min after the propan-2-ol had evaporated. The 0–34 s TEM images mainly show the elimination process of the liquid leveling caused by the immersion of nanopillars in propan-2-ol, and those at 34–79 s show the recovery behavior of the nanopillars. The spaces between nanopillars are designated as areas 1–3 in the TEM image at 0 s. To investigate the correlation between the difference in the liquid level and the amount of nanopillar displacement, we selected an area in

which the interface position had moved significantly. The same observations are also shown in Supplementary Video 3.

Table 1 shows the temporal dependence of the space width of the 3 areas shown in the TEM image at 0 s of Fig. 9. The space widths of all areas approached the original space width of 60 nm. This shows that the collapsed nanopillars recovered, at least partially, on reimmersion in the liquid. However, the value of the space width at 79 s varied from area to area; for example, the space width of regions 1 and 2 at 79 s was more than 60 nm. This indicates that the displacements were not completely recovered, and it is thought that the displacements of nanopillars caused a structural breakdown that resulted in their incomplete recovery.

Table 1. Space widths of Areas 1 to 3 in the six TEM images shown in Fig. 9. The definition of space width is the same as that in Fig. 6.

	Time(sec)	0	3	34	49	64	79
Space width (nm)	Area1	154	146	146	111	88	86
	Area2	173	173	173	143	103	88
	Area3	143	134	131	68	60	57

Figure 10 shows the temporal variation of nanopillar displacement and liquid-surface height in areas 1-3, where there was a large change in the position of the liquid surface. The height of the liquid surface in each area reached almost 600 nm at 34 s, indicating that the nanopillars were almost completely immersed in propan-2-ol at 34 s. On the other hand, the displacement of the space width did not recover during 0 to 34 s, but did recover after 34 s when the nanopillars were immersed in propan-2-ol. This indicates that the recovery of nanopillars occurs in the phase when

the meniscus is eliminated, not in the phase when the difference in liquid level due to capillary interactions is eliminated. It can also be seen that nanopillars started to recover after some time in propan-2-ol. It is necessary to eliminate adhesion between nanopillars in order for them to recover. There are several ongoing studies on the adhesive strength of nanopillars, for example, there are reports that molecules precipitated from liquids are trapped on the adhesive surface.[36,37] We can understand why the nanopillars began to recover after being immersed in the liquid if we assume that adhesion between nanopillars was eliminated by desorption of molecules trapped between nanopillars when the adhesion surfaces were immersed in liquid. It is also important to examine whether a liquid layer remains between the adhesive surfaces; if liquid layer is trapped between the pillars, the adsorption force is likely to be weak. On the other hand, the TEM image at 79 s shows that some nanopillars recovered whereas others did not do so. The cause of this difference is not known at this time, but at least it indicates that the adhesive forces between nanopillars is higher than the elastic forces. To understand the phenomena related to the recovery of nanopillars, it is necessary to verify the complex adhesion mechanism, and this observation method is expected to be applied to the validation of the adhesion model of nanopillars.

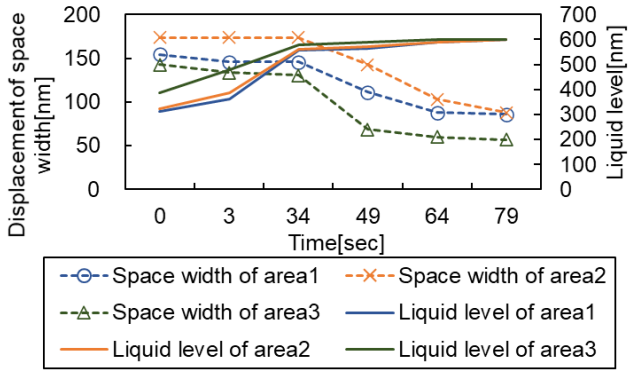

Figure 10. Temporal dependence of the space width and liquid-level height. Areas 1-3 are shown in the TEM images in Fig. 9. The definitions of the space width and the liquid-surface height are the same as in Fig. 6.

CONCLUSION

We observed the collapse behavior of nanopillars caused by propan-2-ol evaporation at the nanoscale and in a cross-sectional view. As a result, the behaviors of the liquid and the collapse of nanopillars induced by the propan-2-ol evaporation were clarified simultaneously, and the conventional model of the collapse of nanopillars by capillary interactions was validated. The collapse behavior of nanopillars was found to occur in two phases. In the first phase, a meniscus is formed between the nanopillars during the drying process from the top to the bottom, and nanopillars collapse due to a difference in capillary forces caused by a difference in the levels of the liquid. In the second step, the liquid pool remaining between the collapsed nanopillars dries from the bottom to the top, and the collapsed state of the nanopillars is maintained by the surface tension of the remaining droplets. In addition, by utilizing the unique function of the Poseidon holder, which allows a liquid to be injected during observation, we observed the recovery behavior of the collapsed nanopillars. We found that nanopillars can recover on reimmersion in liquid, even after they have collapsed.

These observations were obtained for the first time by establishing a method for nanomachining and preparing nanopillars in a solution cell by FIB, without collapsing them. By using this experimental method, it is possible to capture temporal changes in the nanostructure displacement and interfacial migration at the nanoscale. On the other hand, there are challenges. It is necessary to acquire information in the depth direction to permit three-dimensional quantitative analysis. The effect of the electron beam on the dynamics should also be considered. However, if these challenges can be overcome, it should be possible to provide an improved validation of conventional models and to facilitate an understanding of the collapse of nanostructures due to capillary interactions, which hampers the miniaturization of semiconductor devices.

Supporting Information

Supplementary Video 1: The collapse behavior of nanopillars due to evaporation of propan-2-ol. The time and scale are presented in the video.

Supplementary Video2: The evaporation behavior of propan-2-ol between nanopillars. The time and scale are presented in the video.

Supplementary Video3: The recovery behavior of collapsed nanopillars when they were reimmersed in propan-2-ol. The time and scale are presented in the video.

AUTHOR INFORMATION

Corresponding Authors

*E-mail: sasaki@screen.co.jp

*E-mail: ykimura@lowtem.hokudai.ac.jp

ORCID

Yuki Kimura: 0000-0002-9218-7663

Funding Sources

This work was supported by JSPS KAKENHI Grant Numbers JP15H05731 and JP20H05657.

ACKNOWLEDGMENT

We thank the Open Facility, Global Facility Center, Creative Research Institution, Hokkaido University for allowing us to conduct the observation of Si nanopillars by using ALD (R-200 Advanced; Picosun Oy), FIB (Hitachi FB-2100), FIB-SEM (JEOL JEM-9320FIB), and a

micromanipulator (MICRO SUPPORT APS-001R) equipment, and for providing insight and expertise that greatly assisted the research.

REFERENCES

(1) Moore, E. G. Cramming More Components onto Integrated Circuits. *Electronics* **1965**, *38*, 114–117.

(2) Waldrop, M. M. The Chips Are Down for Moore's Law. *Nature* **2016**, *530* (7589), 144‑147.

(3) Yang, C. C.; OuYang, H.; Chen, K. F.; Peng, Y. Y.; Liou, J. W.; Chou, C. C.; Tsai, H. Y.; Lin, K. C.; Jeng, S. M.; Tao, H. J.; Cao, M. Wet Clean Induce Pattern Collapse Mechanism Study. *Solid State Phenom.* **2012**, *187*, 253–256.

(4) Hui, C. Y.; Jagota, A.; Lin, Y. Y.; Kramer, E. J. Constraints on Microcontact Printing Imposed by Stamp Deformation. *Langmuir* **2002**, *18* (4), 1394–1407.

(5) Zhang, Y.; Lo, C.-W.; Taylor, J. A.; Yang, S. Replica Molding of High-Aspect-Ratio Polymeric Nanopillar Arrays with High Fidelity. *Langmuir* **2006**, *22* (20), 8595–8601.

(6) Liu, G.; Ahou, J.; Xiong, Y.; Zhang, X.; Tian, Y. Auxiliary Drying to Prevent Pattern Collapse in High Aspect Ratio Nanostructures. *Nanotechnol.* **2011**, *22* (30), 305305.

(7) Raccurt, O.; Tardif, F.; Arnaud d'Avitaya, F.; Vareine, T. Influence of Liquid Surface Tension on Stiction of SOI MEMS. *J. Micromech. Microeng.* **2004**, *14* (7), 1083−1090.

(8) Sebaai, F.; Vereecke, G.; Xu, X. M.; Baudot, S.; Amemiya, F.; Komori, K.; Holsteyns F. Cleaning of High Aspect Ratio STI Structures for Advanced Logic Devices by Implementation of a Surface Modification Drying Technique. *Solid State Phenom.* **2018**, *282*, 190–193.

(9) Yu, M.; Zhao, S.; Gao, C.; Guo, X.; Xu, X.; Shi, Y.; Jing, Y.; Chen, B. A Novel Method to Overcome Photoresist Collapse with High Aspect Ratio Structures. *Microsyst. Technol.* **2014**, *20*, 2185–2189.

(10) Patel, M. N.; Sirard, S.; Limary, R.; Hymes, D. Freeze Drying of High Aspect Ratio Structures. *Solid State Phenom.* **2015**, *219*, 119–122.

(11) Chen, H. W.; Verhaverbeke, S.; Gouk, R.; Leschkies, K.; Sun, S.; Bekiaris, N.; Visser, R. Supercritical Drying: A Sustainable Solution to Pattern Collapse of High-Aspect-Ratio and Low-Mechanical-Strength Device Structures. *ECS Trans.* **2015**, *69* (8), 119–130.

(12) Bico, J.; Roman, B.; Moulin, L.; Boudaoud, A. Elastocapillary Coalescence in Wet Hair. *Nature* **2004**, *432*, 690.

(13) Py, C.; Bastien, R.; Bico, J.; Roman, B.; Boudaoud, A. 3D Aggregation of Wet Fibers. *Europhys. Lett.* **2007**, *77* (4), 44005.

(14) Cambau, T.; Bico, J.; Reyssat, E. Capillary Rise Between Flexible Walls. *Europhys. Lett.* **2011**, *96* (2), 24001.

(15) Kim, H.; Mahadevan, L. Capillary Rise Between Elastic Sheets. *J. Fluid Mech.* **2006**, *548*, 141–150.

(16) Tawfick, S.; De Volder, M.; Hart, J. A. Structurally Programmed Capillary Folding of Carbon Nanotube Assemblies. *Langmuir* **2011**, *27* (10), 6389–6394.

(17) Wilfinger, R. J.; Chhabra, D. S.: Bardell, P. H. A Frequency Selective Device Utilizing the Mechanical Resonance of a Silicon Substrate. *Proc. IEEE* **1966**, *54* (11), 1589–1591.

(18) Tanaka, T.; Morigami, M.; Atoda, N. Mechanism of Resist Pattern Collapse During Development Process. *Jpn. J. Appl. Phys.* **1993**, *32* (125), 6059–6064.

(19) Namatsu, H.; Kurihara, K.; Nagase, Masao.; Iwadate, K.; Murase, K. Dimensional Limitations of Silicon Nanolines Resulting from Pattern Distortion Due to Surface Tension of Rinse Water. *Appl. Phys. Lett.* **1995**, *66*, 2655–2657.

(20) Yoshimoto, K.; Stoykovich, M. P.; Cao, H. B.; De Pablo, J. J.; Nealey, P. F.; Drugan, W. J. A Two-Dimensional Model of the Deformation of Photoresist Structures Using Elastoplastic Polymer Properties. *J. Appl. Phys.* **2004**, *96*, 1857–1865.

(21) Singh, K.; Lister, J. R.; Vella, D. A Fluid-Mechanical Model of Elastocapillary Coalescence. *J. Fluid Mech.* **2014**, *745*, 621–646.

(22) Chini, S. F.; Amirfazli, A. Understanding Pattern Collapse in Photolithography Process Due to Capillary Forces. *Langmuir* **2010**, *26* (16), 13707–13714.

(23) Chandra, D.; Yang, S. Stability of High-Aspect-Ratio Micropillar Arrays Against Adhesive and Capillary Forces. *Acc. Chem. Res.* **2010**, *43* (8), 1080–1091.

(24) Chandra, D.; Yang, S. Capillary-Force-Induced Clustering of Micropillar Arrays: Is It Caused by Isolated Capillary Bridges or by the Lateral Capillary Meniscus Interaction Force? *Langmuir* **2009**, *25* (18), 10430–10434.

(25) Hadjittofis, A.; Lister, J. R.; Singh, K.; Vella, D. Evaporation Effects in Elastocapillary Aggregation. *J. Fluid Mech.* **2016**, *792*, 168–185.

(26) Pokroy, B.; Kang, S. H.; Mahadevan, L.; Aizenberg, J. Self-Organization of a Mesoscale Bristle into Ordered, Hierarchical Helical Assemblies. *Science* **2009**, *323* (5911), 237–240.

(27) Roman, B.; Bico, J. Elasto-Capillarity: Deforming an Elastic Structure with a Liquid Droplet. *J. Phys.: Condens. Matter* **2010**, *22* (49), 493101.

(28) De Volder, M.; Hart, A. J. Engineering Hierarchical Nanostructures by Elastocapillary Self-Assembly. *Angew. Chem., Int. Ed.* **2013**, *52* (9), 2412–2425.

(29) Grinthal, A.; Kang, S. H.; Epstein, A. K.; Aizenberg, M.; Khan, M.; Aizenberg, J. Steering Nanofibers: An Integrative Approach to Bio-Inspired Fiber Fabrication and Assembly. *Nano Today* **2012**, *7* (1), 35–52.

(30) Chen, B.; Seidel, S.; Hori, H.; Gupta, M. Self-Assembly of Pillars Modified with Vapor Deposited Polymer Coatings. *ACS Appl Mater. Interfaces* **2011**, *3* (11), 4201–4205.

(31) Hu, Y.; Lao, Z.; Cumming, B. P.; Wu, D.; Li, J.; Liang, H.; Chu, J.; Huang, W.; Gu, M. Laser Printing Hierarchical Structures with the Aid of Controlled Capillary-Driven Self-Assembly. *Proc. Natl. Acad. Sci. U. S. A.* **2015**, *112* (22), 6876–6881.

(32) Taroni, M.; Vella, D. Multiple Equilibria in a Simple Elastocapillary System. *J. Fluid Mech.* **2012**, *712*, 273–294.

(33) Vrancken, N.; Ghosh, T.; Anand, U.; Aabdin, Z.; Chee, S. W.; Baraissov, Z.; Terryn, H.; De Gendt, S.; Tao, Z.; Xu, X.; Holsteyns, F.; Mirsaidov, U. Nanoscale Elastocapillary Effect Induced by Thin-Liquid-Film Instability. *J. Phys. Chem. Lett.* **2020**, *11* (7), 2751–2758.

(34) Legtenberg, R.; Tilmans, H.; Elders, J.; Elwenspoek, M. Stiction of Surface Micromachined Structures After Rinsing and Drying: Model and Investigation of Adhesion Mechanisms. *Sens. Actuators, A* **1994**, *43* (1–3), 230–238.

(35) Park, J. E.; Park, S. J.; Urbas, A.; Ku, Z.; Wie, J. J. Programmable Stepwise Collective Magnetic Self-Assembly of Micropillar Arrays. *ACS Nano* **2022**, *16* (2), 3152–3162.

(36) Hu, M.; Ou, F. S.; Wu, W.; Naumov, I.; Li, X.; Bratkovsky, A. M.; Williams, R. S.; Li, Z. Gold Nanofingers for Molecule Trapping and Detection. *J. Am. Chem. Soc.* **2010**, *132* (37), 12820–12822.

(37) Kim, A.; Ou, F. S.; Ohlberg, D. A. A.; Hu, M.; Williams, R. S.; Li, Z. Study of Molecular Trapping Inside Gold Nanofinger Arrays on Surface-Enhanced Raman Substrates. *J. Am. Chem. Soc.* **2011**, *133* (21), 8234–8239